ACTA IMEKO
ISSN: 2221-870X
February 2015, Volume 4, Number 1, 5 - 10

Preliminary study of an ancient earthquake-proof construction technique monitoring by an innovative structural health monitoring system.

Carmelo Scuro[1], Domenico L. Carnì[2], Francesco Lamonaca[3], Renato S. Olivito[4], Gabriele Milani[5]

[1] Department of Physics, University of Calabria, 87036 Rende (CS), Italy
[2] DIMES - Department of Informatics Modelling Electronics and Systems Science, University of Calabria, 87036 Rende (CS), Italy
[3] DING - Department of Engineering, University of Sannio, 82100 Benevento, Italy
[4] DINCI – Department of Civil Engeneering, University of Calabria, 87036 Rende (CS), Italy
[5]Department of Architecture, Built Environment and Construction Engineering, Technical University of Milan, 20133 Milan, Italy

ABSTRACT
The historical and cultural heritage analysis of the Italian territory is of primary importance, because this territory is one of the richest in the world and can enrich our knowledge in different field. In fact, in the field of structural engineering, a new discovery was made in Calabria, in the south of Italy. By investigating various architectural treatises related to earthquake-proof constructions, new knowledge was gained by analyzing buildings made with fictile tubules bricks. One of them is an unprecedented anti-seismic construction widespread in southern Calabria and patented by Pasquale Frezza.
In order to avoid the collapses of these structures, in this work, an innovative method to monitor and obtain the mechanical properties of these structures in real time, minimizing measurement uncertainty is proposed.

Section: RESEARCH PAPER

Keywords: Anti-seismic Technique; Experimental Test; Numerical Analysis; Structural Health Monitoring Systems; Measurement Accuracy.

Citation: Thomas Bruns, Dirk Röske, Paul P.L. Regtien, Francisco Alegria, Template for an IMEKO event paper, Acta IMEKO, vol. 3, no. 1, article 1, January 2014, identifier: IMEKO-ACTA-03 (2014)-01-01

Editor: Paolo Carbone, University of Perugia, Italy

Receivedmonthday, year; **In final form** month day, year; **Published**January2014

Funding: This work was supported by Measurement Science Consultancy, The Netherlands

Corresponding author: Carmelo Scuro, e-mail: carmelo.scuro@unical.it

1. INTRODUCTION

In the safeguarding and prevention of possible collapses of structures of historical interest, the collection of information relating to the quality of construction materials, environmental actions, propensity for an alteration of a single component or of the structure in its entirety caused by loss of strength over time of materials and by accidental events, becomes of fundamental importance [1]-[3].

Structural Health Monitoring systems (SHM), guarantee, for different types of structures, the characterization, identification and detection of the evolution of damage [4]-[8] . In the field of structural monitoring, SHMs systems are made up of two main parts: a data logger that allows the transmission and recording of information, and the acquisition system, which evaluate the different physical quantities [9]. In particular, the main information provided by the SHM systems are: temperature, displacement, strain, acceleration, tensile stress and compressive strength and so on [12]. Usually, SHM systems are placed in structures in a non-invasive way and through a reversible process by using sensors. The latter are placed in very precise control points of the structure to minimize unnecessary costs and information [13],[14]. The useful information acquired by the sensors, after having undergone a check, are used in mathematical numerical models of the structures in order to determine the evolution of possible damage and safety [15]. In recent years, structural monitoring systems have been improved by applying the Internet of Things (IoT) paradigm[16]-[19]. This is due to the fact that in the IoT paradigm, each node is capable of processing, detecting and transmitting data. The information, through an internet connection, is transmitted and stored in a Cloud, and processed by distributed systems made functional by a Big Data paradigm [20].

Safeguarding new discoveries of construction techniques is the ultimate aim of researchers, both for structural engineering and in the field of historic heritage. These structures must be preserved from damage and collapse for future generations. The monitoring of historical buildings in seismic areas is a prevalent issue in Italy because of the richness of its historical cultural heritage that cannot be investigated through invasive tests. Typically, the global structural health monitoring of churches or palaces, is evaluated by dynamic analyses. This type of monitoring allows the mechanical parameters functional to future restoration activities to be obtained and the interaction between the static action and the control of possible changes in behavior to be evaluated. Should the construction techniques be known and the types of masonry be well-defined it is possible to define an interaction model of the structure. In the case of an unknown structure or new structure with no information this is not possible [21]-[23].

Most of the historic anti-seismic constructions of Calabria were built with rubble stone and brick masonry [24], frequently composed of various layers with little or no connection between them, and they were built with various raw materials (bricks, stone or fictile tubules [25],[26]) and usually poor mortars. The paper presents the results of total and partial destructive tests carried out on two replicas of historic masonry specimens constructed in according to the patent of Engineer Pasquale Frezza. A preliminary study is carrying out related to the use of an SHM system to be placed on these ancient anti-seismic structures made from the beginning of 1900s [27]. In particular, the paper will be focused on earthquake-proof wooden frame structures made with common brick and fictile tubules [28]. In the SHM system design particular importance was given to the definition of the mathematical model of the structure for the calculation of the structural solicitations in accordance with Italian technical standards. The possibility of having a well-defined numerical model allows for real-time analysis based on the displacement and stress data recorded during monitoring. This was done by several authors not only in the case of new structures such as bridges [29], but also for the study and construction of large-scale monitoring systems for urban centers [30]-[32].

The paper is organized as follows: preliminarily, the theory of structural mechanics used in order to calculated the shear strength in the specimens was exposed; successively, an experimental test is introduced and the results explained; in section three, the numerical model obtained by software at finite element ABAQUS is proposed; following this, the experimental testbed was described and the measurement accuracy determined, and the conclusions are drawn.

2. LITERATURE CRITERIA FOR THE SHEAR STRENGTH PREDICTION OF PIERS

Several simplified models are proposed in the literature for the descriptions of the damage that may occur in masonry piers. These models are based on the evaluation (not accurately) of the local/mean stress generated by forces applied on pre-identified points/sections of the pier [33]. The most frequent failure modes that occur in piers are rocking/crushing, bed joint sliding and diagonal cracking.

For the Diagonal Cracking failure mode two models are usually adopted to describe it [34],[35]. These models are used to describe different types of masonry and often provide different strength values: Mann and Müller model and Turnšek and Čačovič model. In the Mann and Müller model the limit strength domain is defined by means of "local"-type parameters relating to the individual materials that composed the masonry (mortar and bricks) such as the cohesion and friction coefficient in the mortar joints and the tensile strength of the block of masonry under analysis [34]. These two types of parameter are, generally, obtained experimentally, and the individuation of the cohesion and friction coefficient can be difficult for specific masonry such as that in fictile tubules.

In the Turnšek and Čačovič model, the domain is defined through a single parameter of the material: the tensile strength of the masonry, usually determined by the diagonal compression test [35].

In order to study Diagonal Cracking, it is possible to recognize two main types of model: (I) the model proposed by Mann and Müller, which describes the masonry as a composite material and considers the development of the cracks, separately, along bricks and mortar joints; (II) the model proposed by Turnšek and Čačovič, which considered the masonry as an equivalent isotropic material and described indistinctly the development of damage along principal stress directions [36].

The application of the Mann and Müller formulation to a masonry wall made with bricks and fictile tubules becomes difficult. It is based on two main hypotheses:

(i) the mechanical properties of head joints are negligible, and in the case in question the bricks have a square section;

(ii) bricks are much stiffer than mortar joints, but the tubules are hollow and have a cylindrical conformation, and this hypothesis cannot be satisfied.

For these reasons, it was decided to use the formulation of Turnšek and Čačovič that considers the masonry as an isotropic material. The reference stress σ_c, the maximum principal stress acting at the center of the pier σ_I must not exceed the tensile strength of the masonry f_t. The latter parameter is assumed as constant in any loading direction (isotropic limit stress domain) [37]. This was possible because the authors, in previous works, carried out a homogenization of the material with which the wall was made [38],[39].

The Maximum principal stress at the center of the pier was calculated with the following equation:

$$\sigma_I = \frac{\overline{\sigma_y}}{2} + \sqrt{\left(k_{1d}\,\bar{\tau}\right)^2 + \left(\frac{\overline{\sigma_y}}{2}\right)^2} \tag{1}$$

where: $\bar{\tau}$ and $\overline{\sigma_y}$ are the mean shear and normal stresses acting on the cross-section of the pier and k_{1d} is the ratio of the shear stress at the center of the pier to the mean shear stress [23]. The Failure criteria for masonry piers, represented in the resolved stress plane is shown in Figure 1.

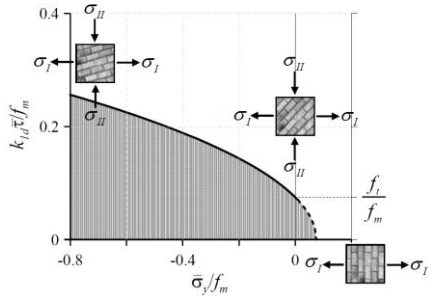

Fig. 1. The Failure criteria of Turnšek and Čačovič for masonry piers, represented in the resolved stress plane [32]

In the new Italian technical standards (document C8.7.1.3.1.1 7/2019) there is a simplification of the formulation of Turnšek and Čačovič in order to obtain the value of shear strength of the masonry pier. Figure 2 shown the schematization adopted of the masonry block.

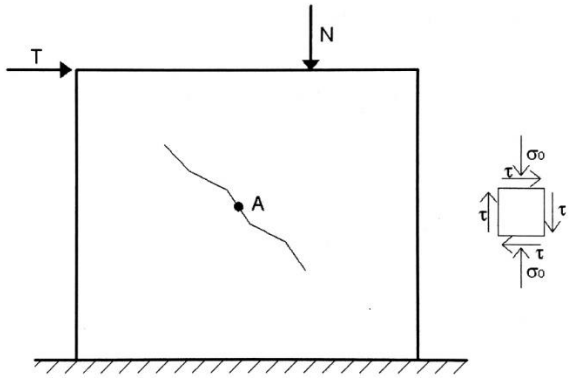

Fig. 2. Schematization adopted of the masonry block.

The normal and tangential stress was calculated at the point A with the following equations:

$$\sigma_0=\frac{N}{l\cdot t} \tag{2}$$

$$\tau_0=\frac{T}{l\cdot t} \tag{3}$$

where T and N are respectively the shear and normal force applied to the masonry block, and l and k are the length and thickness of the masonry. The stress state at point A is represented by Mohr's circle in Figure 3 characterized by center C and radius R, expressed by equation 4 and 5:

$$C=\frac{\sigma_0}{2} \tag{4}$$

$$R=\sqrt{\left(\frac{\sigma_0}{2}\right)^2+\tau^2} \tag{5}$$

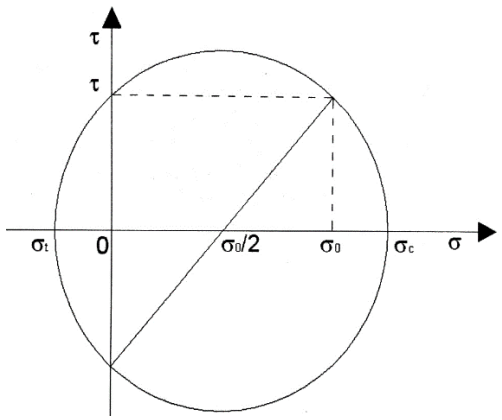

Fig. 3. Tensile state in the point A.

The principal tensile stress that occurred in the masonry is obtained by the following equation:

$$\sigma_t=C-R=\frac{\sigma_0}{2}-\sqrt{\left(\frac{\sigma_0}{2}\right)^2+\tau^2} \tag{6}$$

squaring equation 6 and simplifying, we obtain:

$$\tau^2=\sigma_t^2-\sigma_t\cdot\sigma_0 \tag{7}$$

if - σ_t (tensile stress in the masonry) is equal to f_t, tensile strength of masonry imposed like a limit domain of Turnšek and Čačovič, and $\tau=b\cdot\ \tau_0$, the equation number 7 becomes:

$$\tau_0=\frac{f_t}{b}\sqrt{1+\frac{\sigma_0}{t}} \tag{8}$$

multiplying by the area of the section the shear strength of the masonry pier is obtained:

$$V_s=\frac{f_t\cdot l\cdot t}{b}\sqrt{1+\frac{\sigma_0}{t}}=\frac{1.5\cdot l\cdot t\cdot\tau_{0d}}{b}\sqrt{1+\frac{\sigma_0}{1.5\cdot\tau_{0d}}} \tag{8}$$

Where:

- V_s is the shear strength of the masonry pier obtained for exceeding the limit domain.
- f_t is the tensile strength of masonry.
- b is a coefficient that takes into account the slenderness of the element. It is the ratio between height and length of the pier, its value is in the range between 1 and 1.5.
- τ_{0d} is the reference shear strength

3. EXPERIMENTAL CAMPAIGN

The experimental campaign was conducted in the laboratories of the University of Calabria and was divided into two well-defined steps. Using the same construction process, two masonry walls were made following the patent of Engineer Pasquale Frezza [40]. The first was tested by diagonal compression test and stopped after the specimen collapsed. The second specimen was tested in the same way, but was first damaged and then repaired with Basalt Fiber Reinforced Cementitious Matrix (B-FRCM). After that, the test was repeated until collapse of the reinforced masonry wall.

3.1. Preparation of the specimens

The dimensions of the two specimen walls are 60×60×15 cm^3. The external timber frame is constructed in a carpentry workshop and consists of four poplar beams with a cross-section of 15×5 cm^2 (poplar is a typical wooden building material used for constructions in Calabria). The connection between contiguous beams is ensured by cutting their extremities to make half-lap fastenings and then attaching them with four iron bolts.

After the outer timber frame is built, the inner masonry wall is created. The bricks used have a square cross-section of 5.5 cm per side and a height of 13 cm. The fictile tubules are nomenclating NFTs (New Fictile Tubules) [38],[39] since they are produced in a potter industry with faster and innovative techniques, and then refined on the potter's wheel. They are characterized by the same height as the bricks (13 cm) and are 6 mm thick (Figure 4, Figure 5). The mortar is characterized by a compressive strength of about 2.5 MPa and corresponds to the one labelled as M2.5 *bastarda* according to Table 11.10.IV of the 2008 Italian Building Code. This particular mortar consists of 1 part of cement, 2 of lime mortar and 9 of sand.

The specimen wall is completed by casting a 2 cm thick layer of mortar to cover the tips of the fictile tubules (Figure 6).

Fig. 4. Arrangement of bricks and NFTs in the timber frame.

Fig. 5. Mortar casting.

Fig. 6. Creation of the upper layer of mortar.

3.2. Diagonal compressive test on the first specimen

The diagonal compressive test is carried out by rotating the specimen wall by 45°; two steel caps are placed on the specimen, one at the bottom for support and the other at the top for uniformly distributing the load. The speed of the test is 0.5 mm/s. Two couples of transducers are applied to the masonry specimen to monitor further the relative displacements: those referred to as LVDT0 measure vertical displacements between two bricks, whereas those referred to as LVDT1 measure horizontal displacements between two fictile tubules (Figure 7).

Another transducer that has the same characteristics as those used for calculating the displacements of the masonry, was positioned near the upper part of the load cell in order to measure the lowering of the cross-member of the test machine.

The load-displacement diagram is shown in Figure 8: after a linear elastic branch up to 80% of the maximum load, the diagram displays a decrease in the elastic modulus and reaches a plateau, where the peak load is attained and is equal to 51.48 kN. at this load value, the displacement of the load cell, recorded by the third transducer, is 11.526 mm. The hardening branch is most likely due to friction between mortar and the fictile tubules elements, and to the overall compressive stress state of the specimen wall.

Fig. 7. Set up of the test.

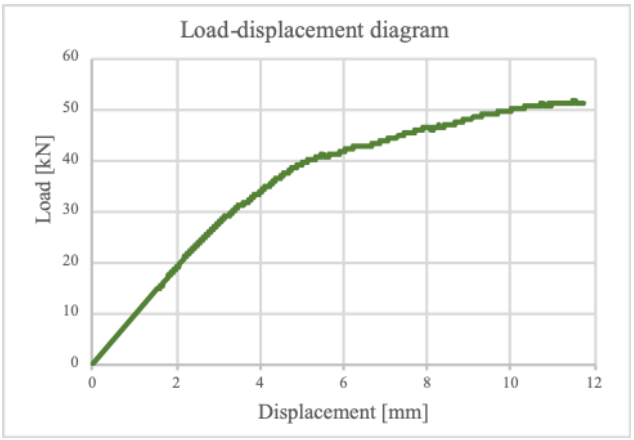

Fig. 8. Load-displacement diagram

The shear strength of the wall S_s is evaluated using equation (9) as suggested by [41]:

$$S_S = \frac{0.707 \cdot P}{A_n} \tag{9}$$

P is the peak load and A_n is the net area which is evaluated according to equation (10):

$$A_n = \left(\frac{w+h}{2}\right) t \cdot n \tag{10}$$

w and h are respectively the width and the height of the specimen (here considered as the dimensions of the masonry inner core and both 50 cm), t is the thickness of the specimen (15 cm) and n is a coefficient related to the rate of voids in the specimen (here considered 0.6 where 1 corresponds to a wall with no voids). The shear strength corresponding to the peak load is 0.81 MPa.

Figure 9 shown the Load Vs Displacement diagrams recording by transducers LVDT and LVDT1 during the test.

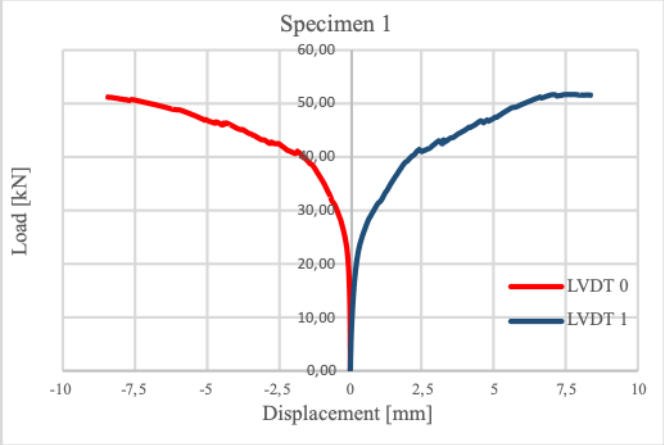

Fig. 9. Load vs Displacement diagrams of transducers for specimen 1

3.3. Diagonal compressive test on the second specimen

The same test set up was used to perform the analyses on specimen number 2. In this case, the test was stopped at the formation of the first damage and when the diagram was arrived at the finish of a linear elastic branch. The recorded peak load is 46.77 kN (Figure 10).

The shear strength of the wall Ss was evaluated using equation (9); the value corresponding to the peak loads is 0.73 MPa.

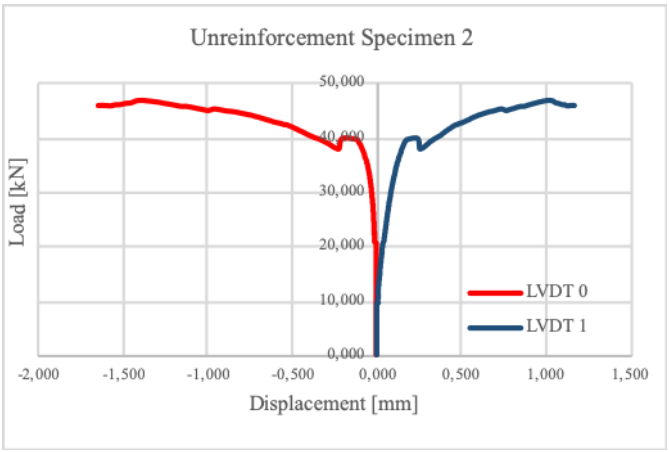

Fig. 10. Load vs Displacement diagrams of transducers for unreinforced specimen 2

When the first damage developed in the specimen, the test was stopped, and the specimen was repaired and reinforced. Three Basalt-FRCM strips of 100 mm were placed at the side of the wall characterized by a layer of two cm of mortar (Figure 11). The B-FRCM is chosen because guarantees compatibility with the support and is characterized by: tensile strength and Young's modulus for basalt fibers of 301.5 MPa and 16 GPa respectively, while those for B-FRCM are 134 MPa and 19 GPa [22]. In order to measure the strains on them, two strain gauges were applied to the central strip in correspondence to the fibers perpendicular to the cracks. Then, the test was repeated on the reinforced specimen until collapse.

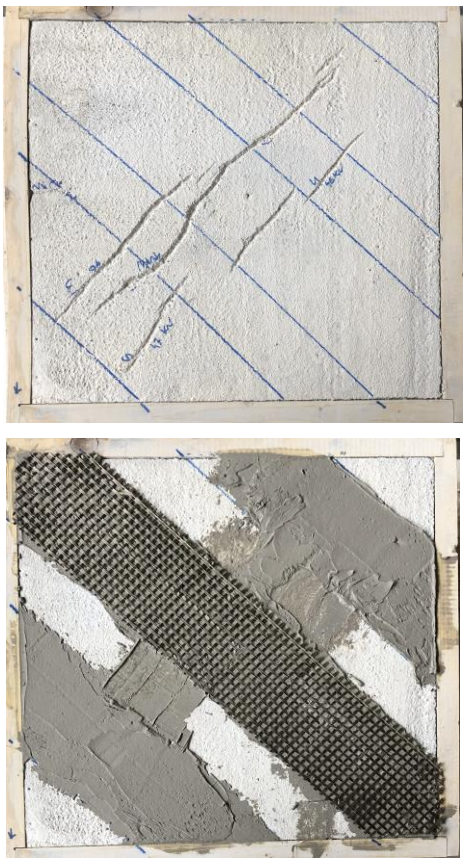

Fig. 11. Specimen 2 before and after reinforcement

The maximum value of the load recorded during the reinforced test was 66.48 kN (Figure 12). At this load value, a failure of the Basalt-FRCM (B-FRCM) reinforcement occurred [42],[43]. The collapse of the reinforcement strip happens through debonding with the cohesive failure of the substrate (Figure 13).

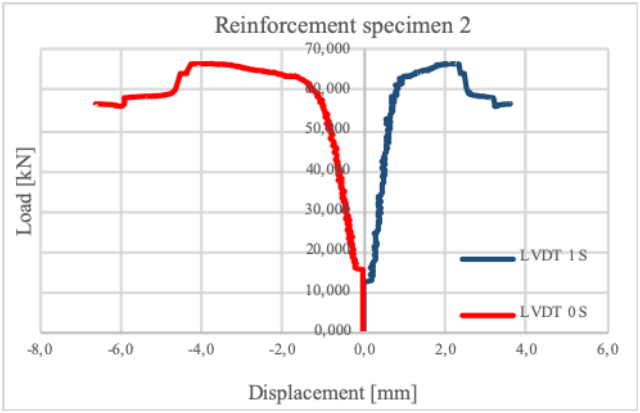

Fig. 12. Load Vs Displacement diagrams of transducers for reinforcement specimen 2

In order to obtain the value of the strain that occurred in the reinforced basalt fiber during the test, two strain gauges were applied to the central part of the diagonal BFRP.

A strain gauge is a device commonly used in order to obtain the strain on a specimen subject to different type of stress, for example compression or tensile stress.

Fig. 13. Collapse of the reinforcement strip

The strain gauges employed in the test are the most common type and consists of an insulating flexible backing which supports a metallic foil pattern. The gauge is positioned on the strip of B-FRCM with a cyanoacrylate. When the basalt fibers are deformed, the foil is deformed, causing its electrical resistance to change. This resistance change, usually measured using a Wheatstone bridge, is related to the strain by the quantity known as the Gauge factor.

Figure 14 shown the diagram Shear Stress Vs Strain obtained during the test conducted on the reinforced specimen.

The Shear Stress was evaluated by equation 9 and in this case is 1.04 MPa.

The average value of the strain recorded during the test by the two strain gauges was 3.25 [μm/m] E-3. This value is in accordance with the value prescribed by the manufacturer of the fiber that certifies it in the range 3- 3.5 [μm/m] E-3.

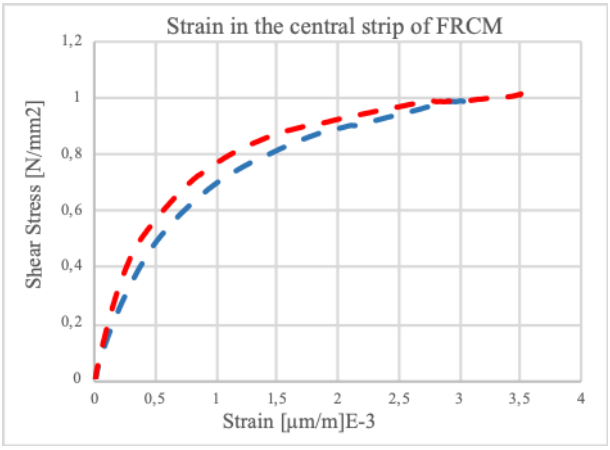

Fig. 14. Shear Stress Vs Strain

4. NUMERICAL MODEL

The principal goal in the creation of the numerical model is that of repeating the diagonal compressive test and simulating the behaviour of these structures. The commercial CAD software Rhinoceros was employed in order to create a simplified geometrical model of the specimen. The outer timber frame, the common bricks, the fictile tubules are modelled apart like a solid composed of a surface characterized by a normal vector facing out [44]. After that, the single part is assembled and imported together into the commercial FE software Abaqus, where the analysis is conducted.

The common brick and the timber frame are meshed using hexahedral C3D8 finite elements (classified C3D8 in Abaqus), while tetrahedral elements (C3D4) are used for the fictile tubules and inner mortar. The final model created is composed of a total of 47093 nodes and 165710 elements (1120 C3D8 and 164590 C3D4) [25],[38]. In order to calculate the behaviour of their bond, a tie constraint is imposed between the mortar and the fictile tubules and bricks. a general contact is imposed to simulate the interaction between the timber frame and the mortar, imposing a friction coefficient of 0.8 [45].

The material of common bricks and timber frame is modelled like linear elastic material, specifically, the orthotropy of the wood is not considered, but this is imposed as an isotropic material in order to simplify the final model and reduce the computational burden [46]. It is possible because, during the experimental test, the timber frame is damaged after the mortar and does not arrived at collapse. Instead, fictile tubules and mortar are simulated using CDP material model (Concrete Damaged Plasticity), available in the Abaqus library. Originally, the CDP was created to simulate the behaviour of concrete under fairly low confining pressure, considering the damage that develops in it, its general formulation allows its use in the simulation of a broader range of materials [47]-[49]. Table 1 lists Young's moduli and Poisson's ratios for the four materials here considered. Table 2 and Table 3 display the tensile constitutive law for fictile tubules and mortar, respectively, expressed in terms of displacements and stresses.

Table 1 Values of Young's modulus and Poisson's ratio.

Material	Young's modulus [MPa]	Poisson's ratio [-]
Wood	270	0.00
Clay (bricks)	1290	0.15
Clay (tubules)	4800	0.15
Mortar	275	0.20

Table 2 Tensile constitutive law for mortar.

Tensile stress [MPa]	Plastic displacement [mm]
0.4200	0.00
0.0005	0.03
0.0005	6.50

Table 3 Tensile constitutive law for tubules' clay.

Tensile stress [MPa]	Plastic displacement [mm]
2.7500	0.000
0.0005	0.058
0.0005	10.75

The ultimate displacement of the materials is imposed with a high value in order to complete successfully the analysis without affecting the structural response of the materials. A damage parameter of 0.99 is set for both mortar and the clay of the tubules in proximity of a plastic displacement of 0.03 mm.

The comparison between the numerical and experimental load-displacement diagrams is shown in Figure 15. The numerical analysis satisfactorily estimates the linear elastic branch of the graph, but the peak load attained is 8% higher than the experimental one (55.54 kN against 51.48 kN). Also, the numerical analysis halts for an ultimate displacement which is close to that related to the load peak recorded during the experimental test. In fact, the displacement obtained by the numerical model is 11.700mm, the experimental one 11.526 mm.

The damage in the numerical model corresponds to the experimental outcome, while displaying more cracks at the top and four single cracks departing from the midsection of each timber beam. Given the overall fair correspondence in terms of

crack patterns, it can be assumed that these four single cracks appear only for numerical reasons, therefore they play no effective role in the overall response of the numerical model (Figure 16).

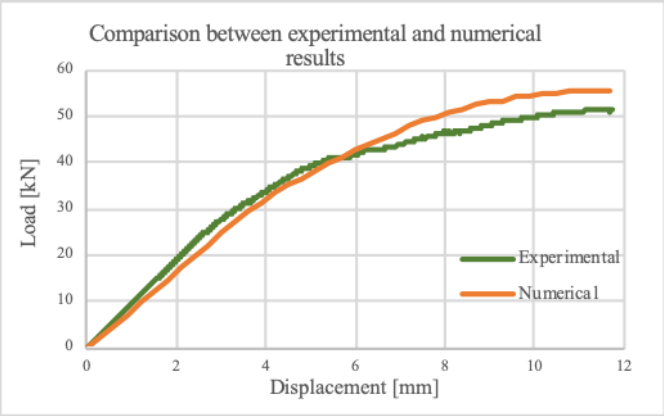

Fig. 15. Shear Stress Vs Strain

5. EXPERIMENTAL TESTBED AND MEASUREMENT ACCURACY

Two different Acquisition System (AS) were used in order to monitor the displacements, in the case of first specimen, and the displacement and the strain of the basalt fibber in the case of the second specimen.

The first AS was composed as follows: three Linear Variable Differential Transformers (LVDT) [46], used for monitoring the horizontal and vertical displacement, were connected to a data acquisition system (DAQ) Spider-8 which transmitted the data to a computer. The second was composed of two LVDT and two strain gauges, which were connected to a DAQ 5100B of System Micromeasurement. The second DAQ permits the acquisition, in real time, of two different types of data that were transmitted to a computer in order to process them in real time.

The LVDTs used to monitor the displacement in the masonry wall are the WA-T 50 mm type and are procured by HBM. The displacement transducers WA-T are in probe version and they use an active quarter bridge circuit based on the differential inductor principle. The bridge is also directly integrated in the sensor to create a full bridge circuit for easy connection of the WA-T transducer to DAQ.

Figure 16. Comparison of cracks development in in the back and front side of numerical model and experimental specimen wall.

The linearity variation in relation to nominal value is ±1% range of displacement that it is possible to measure with this type of LVDTs is 0-50 mm [51].

The DAQ, Spider 8, was used by an individual operator and has ensured: Simultaneous measurement acquisition, high sampling rate at 16-bit resolution and selectable digital filters. The linearity variation in relation to nominal value is ±0.05 %.

System 5000's Model 5100B Scanners acquire test data within 1 millisecond from up to 1200 channels at scan intervals as short as 0.02 s. This permits to have more accurate test results, and the ability to capture data under static loading conditions immediately before failure of the structure monitored. The Strain gauge cards integrated, include built-in bridge completion for quarter and half bridges, and a constant voltage power supply for 0.0, 0.5, 1.0, 2.0, 5.0, and 10.0 VDC bridge excitation. The A/D CONVERTER is characterized by 16-bit successive approximation converter with 40 µs total conversion time per reading [52].

The 5100B operate with 1 ms per scan. Fifty complete scans per second typical usage. Concurrent scanning for all scanners. Input channels in each single scanner are scanned sequentially at 0.04 ms intervals and stored in random access memory within a 1 ms window.

The strain gauges employed are the PFL-10-1 type. They are Polyester linear gauges with mild steel compensation. This is a foil strain gauge with a polyester resin backing. This type of strain gauge is characterized by 2 cm lead wires pre-attached, a Strain Limit of 2 % (20000 µstrain), operational temperature [20, 80] °C and nominal resistance of 120 Ω.

The main problem detected during the second test on the second specimen was the return of the LVDT data.

As shown in figure 12 in the elastic branch of the Load Vs Displacement diagram there is a disturbance caused by a noise due to the DAQ. The data acquired instead by the channels dedicated to the strain gauges do not present this problem. For this reason, a spline fitness function was implemented to minimize the effect of the noise preserving the linearity of the Load Vs Displacement graphs, obtaining new diagrams shown in Figure 17. In particular, a cubic spline interpolation algorithm is used on the data acquired. The spline function smooths the random trend due to the noise, permitting highlighting the trend of the load vs the displacement.

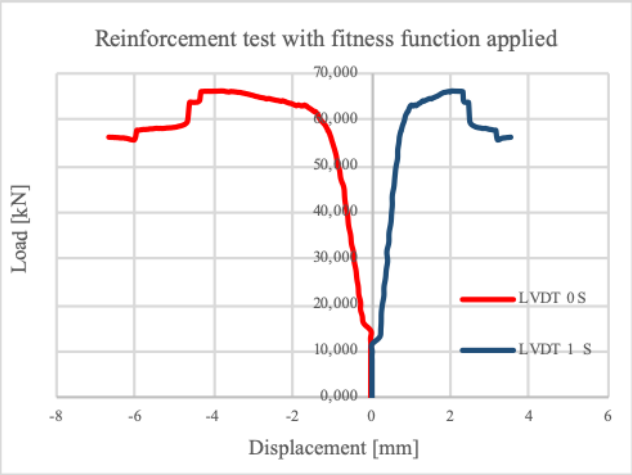

Fig. 17. Load vs Displacement diagrams after the application of fitness function

The linearity variation in relation to the nominal value of the DAQ is ±0.05 %, as a consequence it is negligible in the evaluation of the measurement accuracy with respect to the sensor linear characteristic. Instead, taking into consideration the linearity variation in relation to the nominal value for the LVDTs is ±0.500 mm [53],[54]. This value must be reduced by dividing by √3 and identify a range of ±0.288 mm [55]-[60].

6. CONCLUSION

The principal aim of the paper is a preliminary research into the reliability and monitoring under dynamic loads of the technique patented by Pasquale Frezza. This type of anti-seismic construction consists of masonry walls built with bricks and fictile tubules, arranged in staggered and alternating manner, all contained in a timber wooden frame.

For the first specimen, tested until collapse, the experimental diagonal compression tests result in shear strengths of 0.81 MPa and the lowering displacement recorded of the steel plate of the testing machine is 11.526 mm. The second masonry wall was subjected to diagonal compression tests in two distinct phases. The specimen was first damaged, stopping the test when the first cracks appear, and then, it was repaired with B-FRCM and the test was repeated until collapse. The shear strengths obtained are respectively 0.73 MPa and 1.04 MPa. These results highlight how after the strengthening of the second specimen with B-FRCM, the shear strength registered an increase of 43% with respect to the unreinforced case, which points out the importance of fiber reinforcement for increasing the load-bearing capacity also in this kind of structure. However, both values are higher than the usual ones obtained for common masonry walls, and the cracks that formed are consistent with those expected from this type of test.

Figures 18 show the location of the cracks developed during the test of the first specimen at the attainment of the maximum load. On both sides of the masonry wall the cracks develop through mortar, parallel to each other and to the direction of application of the load, barely involving the fictile tubules. The numerical simulation shows good correspondence in terms of load-displacement diagram, with some minor discrepancies, and a development of cracks fairly mirroring the one obtained through the experimental test. In addition, the simulation of the damage in the wall obtained by means of a numerical model, corresponds discreetly to the experimental result. It shows more cracks at the top and four single cracks departing from the middle section of each timber beam. Overall, the model is very similar to the real one and the four cracks mentioned above appear, albeit small, in the back of the wall.

The displacement of the upper plate of the testing machine obtained with the numerical model was compared with the experimental results to evaluate their compatibility. The linearity variation of the LVDT measurement with respect to their nominal values is ±0.288 mm. In the experimental case, the measured displacement is 11.526 ±0.866 mm, and the cover coefficient is 3. The displacement estimated by the numerical model is compatible with the experimental tests (11.700 mm).

The Acquisition system proposed was composed by Linear Variable Differential Transformer (LVDT), used for monitoring the horizontal and vertical displacement, and strain gauges, used for monitoring the strain. These transducers were connected to a data acquisition system (DAQ) Spider-8 which transmitted the data to a computer. All the data acquired are processed in real time with a spline fitness function in order to remove the disturbance caused by a noise due to the DAQ. In addition, a numerical model for these particular construction

techniques was created in order to start real-time analysis relating to the data recorded by the SHM system.

ACKNOWLEDGEMENT

The authors thank the engineers of "NGT Test "laboratory Gennaro Angotti, Cinzia Angotti e Dino Padula for the support in the tests.

REFERENCES

[1] F. Lamonaca, P. F. Sciammarella, C. Scuro, D. L. Carnì and R. S. Olivito, Internet of Things for Structural Health Monitoring, 2018 Workshop on Metrology for Industry 4.0 and IoT, Brescia, Italy, 2018, pp. 95-100.

[2] R.S. Olivito, S. Porzio, C. Scuro, D.L. Carnì, F. Lamonaca, SHM systems applied to the built heritage inventory at the territorial scale. A preliminary study based on CARTIS approach. IMEKO TC-4 International Conference on Metrology for Archaeology and Cultural Heritage Florence, Italy, 2019, pp. 53-58.

[3] A. Barontini, M.G. Masciotta, L.F. Ramos, P. Amado-Mendes, P.B. Lourenço. An overview on nature-inspired optimization algorithms for Structural Health Monitoring of historical buildings. Procedia engineering, 199, (2017), pp. 3320-3325.

[4] C.R. Farrar, K. Worden, An introduction to structural health monitoring, Philosophical Transactions of the Royal Society of London A: Mathematical, Physical and Engineering Sciences, 365, (2007), pp. 303-315

[5] F.Lamonaca, et al., Improved Monitoring of Acoustic Emissions in Concrete Structures by Multi-Triggering and Adaptive Acquisition Time Interval, Measurement, vol.59, (2015), pp.227-236.

[6] D.L. Carni, D. Grimaldi, F. Lamonaca, "Distortion Characterization of Exponential Signal Reconstructed by Low-Chirp Signal", IEEE Transactions on Instrumentation and Measurement, vol.8, No.4, 2019, pp. 980-986.

[7] F.Lamonaca, A.Carrozzini, D.Grimaldi, R.S.Olivito, Acoustic Emission Monitoring of Damage Concrete Structures by Multi-Triggered Acquisition System, Proc.of I2MTC 2012– IEEE International Instrumentation and Measurement Technology Conference, Graz, Austria, 13-16 May, (2012), pp.1630-1634.

[8] C. Scuro, et al., Fictile tubules: A traditional Mediterranean construction technique for masonry vaulted systems. Construction and Building Materials, 193, (2018), pp. 84-96.

[9] X.-H. Zhang, Y.-L. Xu, S. Zhu, S. Zhan, Dual-type sensor placement for multi-scale response reconstruction, Mechatronics, 24 (4) (2014), pp. 376-384.

[10] V.Nastro, et al., "Passive and active methods for Radon pollution measurements in historical heritage buildings", Measurement, vol.114, 2018, pp.526-533.

[11] F. Lamonaca, et al., Monitoring of Environmental Parameters and Pollution by Fungal Spores in the National Gallery of Cosenza: a Case of Study, Measurement, vol.47, (2014), pp.1001-1007.

[12] C. Scuro, P.F. Sciammarella, F. Lamonaca, R.S. Olivito, D.L. Carnì, IoT for structural health monitoring. IEEE Instrumentation & Measurement Magazine, 21(6), (2018), pp. 4-14.

[13] X.-H. Zhang, Y.-L. Xu, S. Zhu, S. Zhan, Dual-type sensor placement for multi-scale response reconstruction, Mechatronics, 24 (4), (2014), pp. 376-384.

[14] F. Lamonaca, et al., Structural Health Monitoring System for Masonry Historical Construction, Proc. of International Conference on Metrology for Archaeology and Cultural Heritage METROARCHEO 2018, Cassino, Italy - October 22-24, 2018.

[15] A. Pierdicca, F. Clementi, D. Isidori, E. Concettoni, C. Cristalli, S. Lenci, Numerical model upgrading of a historical masonry palace monitored with a wireless sensor network, International Journal of Masonry Research and Innovation, 1(1), (2016), pp. 74-98.

[16] P. Daponte, et al., A Survey of Measurement Applications Based on IoT, Proc. of IEEE International Workshop on Metrology for Industry 4.0 and IoT, Brescia, Italy, 16-18 April (2018), pp. 1-6.

[17] I. Tudosa, et al., "Hardware Security in IoT era: the Role of Measurements and Instrumentation", proc. of Int. Workshop on Metrology for Industry 4.0 and IoT (MetroInd4.0&IoT), pp.285-290.

[18] I. Tudosa, et al., "A Flexible DAQ Hardware Architecture using SoCs for IoT based Structural Health Monitoring Systems", proc. of IEEE International Workshop on Metrology for Industry 4.0 and IoT, MetroInd 4.0 and IoT 2019, pp.291-295.

[19] E. Balestrieri, et al., Research challenges in measurements for Internet of Things systems, ACTA IMEKO, 2018, vol 7, N. 4, pp.82 – 94.

[20] R. Kitchin, Big Data, new epistemologies and paradigm shifts. Big data & society, 1(1), (2014).

[21] E. Poletti, G. Vasconcelos, Seismic behaviour of traditional timber frame walls: experimental results on unreinforced walls. Bull Earthquake Eng, 13, (2015), pp.885–916.

[22] E. Poletti, G. Vasconcelos, J.M. Branco, A.M. Koukouviki, Performance evaluation of traditional timber joints under cyclic loading and their influence on the seismic response of timber frame structures. Construction and Building Materials, 127, (2016), pp. 321-334.

[23] G. Vasconcelos, E. Poletti, E. Salavessa, A.M. Jesus, P.B: Lourenço, P. Pilaon, In-plane shear behaviour of traditional timber walls, Engineering Structures, 56, (2013), pp.1028-1048.

[24] R.S. Olivito, R. Codispoti, C. Scuro, A seismic analysis for masonry constructions: The different schematization methods of masonry walls. In AIP Conference Proceedings, Vol. 1906, No. 1, 2017, p. 090007. AIP Publishing LLC.

[25] S. Tiberti, C. Scuro, S. Porzio, G. Milani, R.S. Olivito, Post-Cracking B-FRCM Strengthening of a Traditional Anti-Seismic Construction Technique (Casa baraccata): Extensive Experimental Investigations. In Key Engineering Materials, 817, (2019). pp. 634-641.

[26] G. Vivenzio, Istoria e teoria de' tremuoti in generale ed in particolare di quelli della Calabria, e di Messina del 1783. Stamperia Regale, 1783, Naples.

[27] S.Tiberti, C.Scuro, R.Codispoti, R.S.Olivito, G.Milani.. Experimental and numerical analysis of historical aseismic construction system. In Structural Analysis of Historical Constructions, 2019, pp. 910-918. Springer, Cham.

[28] C. Scuro, D.L. Carnì, F. Lamonaca, R.S. Olivito, G. Milani, An innovative structural health monitoring system for the preliminary study of an ancient anti-seismic construction technique. IMEKO TC-4 International Conference on Metrology for Archaeology and Cultural Heritage Florence, Italy, 2019, pp. 43-47.

[29] L. Marcheggiani, F. Clementi, A. Formisano. Static and dynamic testing of highway bridges: a best practice example. Journal of Civil Structural Health Monitoring, 10(1), (2020), pp. 43-56.

[30] A. Formisano, G. Di Lorenzo, L. Krstevska, R. Landolfo. Fem Model Calibration of Experimental Environmental Vibration Tests on Two Churches Hit by L'Aquila Earthquake. International Journal of Architectural Heritage, (2020). pp.1-19.

[31] G. Di Lorenzo, A. Formisano, L. Krstevska, R. Landolfo. Ambient vibration test and numerical investigation on the St. Giuliano church in Poggio Picenze (L'aquila, Italy). Journal of Civil Structural Health Monitoring, 9(4), (2019), pp. 477-490.

[32] A. Formisano, L. Krstevska, G. Di Lorenzo, R. Landolfo. Experimental ambient vibration tests and numerical investigation on the Sidoni Palace in Castelnuovo of San Pio (L'Aquila, Italy). Int. J. Masonry Research and Innovation, 3(3), (2018), pp. 269.

[33] C. Calderini, S. Cattari, S. Lagomarsino, In-plane strength of unreinforced masonry piers, Earthquake Engineering and Structural Dynamics, 38(2), (2009), pp. 243-267.

[34] W. Mann, H. Müller, Failure of shear-stressed masonry – An enlarged theory, tests and application to shear-walls". Proc. of the International Symposium on Load bearing Brickwork, London, (1980), pp. 1-13.

[35] V. Turnšek, F. Čačovič, Some experimental results on the strength of brick masonry walls, Proc. of the 2nd International Brick Masonry Conference, Stoke-on-Trent, (1970), pp. 149-156.
[36] C. Calderini, S. Cattari, S. Lagomarsino, Identification of the shear mechanical parameters of masonry piers from diagonal compression test. In 11th Canadian Masonry Symposium, Toronto, Canada, 2009.
[37] C. Calderini, S. Cattari, S. Lagomarsino, The use of the diagonal compression test to identify the shear mechanical parameters of masonry. Construction and building materials, 24(5), (2010), pp. 677-685.
[38] C. Scuro, S. Tiberti, R. Codispoti, G. Milani, R.S. Olivito, Fictile tubules: A traditional Mediterranean construction technique for masonry vaulted systems. Construction and Building Materials, 193, (2018), pp. 84-96.
[39] S. Tiberti, C. Scuro, R. Codispoti, R.S. Olivito, G. Milani, Masonry structures built with fictile tubules: Experimental and numerical analyses. In AIP Conference Proceedings, Vol. 1906, No. 1, (2017). p. 090010). AIP Publishing LLC.
[40] P. Frezza, (1909), Construction System of Earthquake-Resistant Houses. Italian Patent 103254
[41] American Society for Testing and Materials (2015) ASTM E519 / E519M-15, Standard Test Method for Diagonal Tension (Shear) in Masonry Assemblages. doi: 10.1520/E0519_E0519M-15
[42] R.S. Olivito, R. Codispoti, C. Scuro, S. Porzio, Experimental evaluation of the adhesion of a FRCM-tuff strengthening system. Procedia Structural Integrity, 12, (2018), pp. 594-601.
[43] R.S. Olivito, R. Codispoti, C. Scuro, Experimental analysis on adhesion of NFRCM Systems applied to masonry structures, In AIMETA 2017 XXIII Conference the Italian Association of Theoretical and Applied Mechanics, Salerno, Italy, 2017, pp. 4-7.
[44] B. de Vries, J.M. Harink, Generation of a construction planning from a 3D CAD model. Automation in Construction, 16(1), (2007), pp.13-18.
[45] P.B. Lourenço, Recent Advances in Masonry Structures: Micromodelling and Homogenisation, in: U. Galvanetto, M.H.F. Aliabadi (Eds.), Multiscale Modeling in Solid Mechanics: Computational Approaches, Imperial College Press, London, United Kingdom, 2009, pp. 251-294.
[46] P. Lonetti, A. Pascuzzo, A. Davanzo, Dynamic behavior of tied-arch bridges under the action of moving loads. Mathematical Problems in Engineering, 2016, (2016), pp 17.
[47] S. Tiberti, M. Acito, G. Milani, Comprehensive FE numerical insight into Finale Emilia Castle behavior under 2012 Emilia Romagna seismic sequence: Damage causes and seismic vulnerability mitigation hypothesis, Engineering Structures, 117, (2016), pp. 397-421.
[48] A. Hillerborg, M. Modéer, P.E. Petersson, Analysis of Crack Formation and Crack Growth in Concrete by Means of Fracture Mechanics and Finite Elements, Cement and Concrete Research, 6 (6), (1976), pp. 773-781.
[49] J.G. Rots, J. Blaauwendraad, Crack Models for Concrete, Discrete or Smeared? Fixed, Multi-Directional or Rotating?, HERON 34 (1) (1989).
[50] P.Antunes, H.Lima, H.Varum, P.André. Optical fiber sensors for static and dynamic health monitoring of civil engineering infrastructures: Abode wall case study, Measurement: Journal of the International Measurement Confederation, 45 (7), (2012), pp. 1695-1705.
[51] HBM LVDT WA-T Data sheet
[52] HBM Spider-8 Data sheet.
[53] Guide to the Expression of Uncertainty in Measurement (GUM) (BIPM, IEC, IFCC, ILAC, ISO, IUPAC, IUPAP, and OIML) ISBN 92-67-10188-9, 1993.
[54] A. Katsuki, T. Sajima, H. Murakami, A.M. Hazrat, O. Ohnishi, K. Akashi, Development of a laser-guiding-type deep small-sized hole-measurement system: Measurement accuracy. Precision Engineering, 63, (2020), pp.18-32.
[55] S. Shi, B. Muralikrishnan, V. Lee, D. Sawyer, Methods to improve the dimensional measurement accuracy of a motion tracking system. Optics and Lasers in Engineering, 130, (2020),106092.
[56] C. Scuro, F. Lamonaca, R. Codispoti, D.L. Carnì, R.S. Olivito, Experimental and numerical analysis on masonry arch built with fictile tubules bricks. Measurement, 130, (2018), pp.246-254.
[57] F. Lamonaca, P.F. Sciammarella, C. Scuro, D.L. Carnì, R.S. Olivito. Synchronization of IoT layers for structural health monitoring. In 2018 Workshop on Metrology for Industry 4.0 and IoT, Brescia, Italy. (2018, April). (pp. 89-94). IEEE.
[58] F. Lamonaca, et al., Preserving Synchronization Accuracy from the Plug-in of Non Synchronized Nodes in a Wireless Sensor Network, IEEE Transactions on Instrumentation and Measurement, vol. 66, (2017), pp. 1058-1066.
[59] D.L.Carni, et al., "From distributed measurement systems to cyber-physical systems: A design approach", Computing International Scientific Journal, vol. 16, 2017, p. 66-73.
[60] F. Lamonaca, C. Scuro, P.F. Sciammarella, R.S. Olivito, D. Grimaldi, D.L. Carnì, A layered IoT-based architecture for a distributed structural health monitoring system. Acta Imeko, 8(2), (2019).